

H U M B O L D T - U N I V E R S I T Ä T Z U B E R L I N



Lebenswissenschaftliche Fakultät

Institut für Biologie

Bachelorarbeit

zum Erwerb des akademischen Grades Bachelor of Science

Titel:

Exploring growth and division of *S.cerevisiae* in a single cell based population model

vorgelegt von

Louis Pascal Polczynski

Matrikelnummer: 576614

E-Mailadresse: polczynl@hu-berlin.de

Geburtsdatum/-ort: 24.10.1996/Berlin

Erstprüferin: Prof.Dr.Dr.h.c., Edda Klipp

Zweitprüfer: Prof.Dr., Uwe Ohler

Datum: 18.02.2021

Abstract

Saccharomyces cerevisiae (budding yeast) is a common model organism. Main reasons are its easy cultivation, relatively small genome and yet distinctive eukaryotic architecture. Its pattern of growth and cell division are two features of widespread interest and extensive experimental research has been performed on the subject. The development of mathematical models can help to gain new insights into the underlying mechanisms of cellular life and ideally direct experimental efforts.

In this thesis two existing models from the same research group have been combined in a new merged model, to benefit from their respective advantages and allow the exploration of new experimental set ups *in silico*.

In 2019 Altenburg et al. published a model to describe the growth and dynamics of budding yeast cell walls [1] as a result of thermodynamic pressures. While performing well within its boundaries, it left space for expansion. Namely it covered only one generation and the timing of budding events was hardwired. In the course of this project it was expanded to cover multiple generations and a module for active cell cycle regulation has been integrated. While the cell grows, it divides and forms daughter cells. Continuing the simulation of these new cells allows the creation of diverse *in silico* populations.

Both the regulatory mechanism used and the framework for population simulations was based on another model for budding yeast. It was first published by Spießer et al. in 2012 [14] and aimed directly at simulating whole populations of individually growing and dividing cells. In contrast to the extended model based on Altenburg et al. as presented here it used a different approach to single cell growth, a so called self-replicator. In the last section of this thesis key results of both models were compared and core mechanisms

evaluated.

Saccharomyces cerevisiae (Bäckerhefe) ist ein häufig genutzter Modellorganismus. Dies hat seine Ursache in der einfachen Kultivierung und dem, gemessen an anderen Eukaryoten, recht kleinen Genom. Das Zusammenspiel von Wachstum und Zellteilung in Hefezellen war in den letzten Jahrzehnten Gegenstand intensiver Forschung. Die Entwicklung mathematischer Modelle kann dazu beitragen zu grundlegende biologische Mechanismen zu verstehen und idealerweise experimentelle Bemühungen fokussieren.

In der hier vorliegenden Arbeit wurden zwei bereits existierende Modelle vereint, um von den jeweiligen Vorteilen zu profitieren und die Simulation neuer *in silico* Experimente zu ermöglichen. Altenburg et al. hatten 2019 ein Modell veröffentlicht, welches das Wachstum der Zellwand von Hefezellen als ein Ergebnis thermodynamischer Prozesse beschrieb [1]. Trotz guter Resultate innerhalb des angedachten Rahmens, hat es Raum für Erweiterungen gelassen. Insbesondere deckte es nur fixe Zeitspannen von einer Zellgeneration ab. Im Laufe dieses Projektes wurde es für die Simulation von mehreren Zellzyklen erweitert und eine aktive Regulation der Generationsdauern implementiert. Die so modellierte Hefezelle bildet in jeder Generation neue Tochterzellen, welche wiederum neue Zellen bilden, sofern man sie als Startpunkt weiterer paralleler Simulationen nutzt. Auf diese Art entsteht eine ganze *in silico* Kultur von Zellen.

Sowohl der Mechanismus für die Regulation der Zellzyklusdauer als auch die Umgebung für die Populationssimulation basieren auf einem weiteren Hefemodell. Dieses wurde in einer ersten Fassung 2012 von Spießer et al. veröffentlicht und zielte direkt auf die Simulation von Kulturen unabhängiger Einzelzellen ab [14]. Im Gegensatz zu dem auf Altenburg et al. basierenden, hier erweiterten Modell, nutzte es einen anderen Ansatz um das Wachstum von Einzelzellen zu beschreiben, einen so genannten Self-Replicator. Im letzten Abschnitt dieser Arbeit werden Hauptresultate beider Modelle miteinander verglichen und Kernmechanismen ausgewertet.

Declaration

Hiermit erkläre ich, dass ich die vorliegende Arbeit selbständig verfasst habe und sämtliche Quellen, einschließlich Internetquellen, die unverändert oder abgewandelt wiedergegeben werden, insbesondere Quellen für Texte, Grafiken, Tabellen und Bilder, als solche kenntlich gemacht habe.

Ich versichere, dass ich die vorliegende Abschlussarbeit noch nicht für andere Prüfungen eingereicht habe.

Mir ist bekannt, dass bei Verstößen gegen diese Grundsätze ein Verfahren wegen Täuschungsversuchs bzw. Täuschung gemäß der fachspezifischen Prüfungsordnung und/oder der Fächerübergreifenden Satzung zur Regelung von Zulassung, Studium und Prüfung der Humboldt-Universität zu Berlin (ZSP-HU) eingeleitet wird.

Berlin, 18.02.2021

Louis Pascal Polczynski

Acknowledgements

I want to thank Edda Klipp for supervising this thesis, as much as Stephan Adler and Björn Goldenbogen for their guidance and patients throughout the project. Furthermore I want to thank Gabi Schreiber and Judith Wodke. A special thanks goes to Karsten Tabelow and Friedrich Putkammer, who's feedback and encouragement on the writing was very helpful. Last but not least I thank both my parents for their love and support and all the opportunities they have given me in life.

Contents

1	Introduction	8
1.1	Motivation	8
1.2	The cell cycle of yeast	9
1.3	The biomass growth model	11
1.4	The volume growth model	14
2	The merged model	18
2.1	Expanding the VGM to multiple generations	18
2.1.1	Coupled implementations	19
2.1.2	Decoupled implementation	29
2.2	Cell cycle regulation	31
2.2.1	Biomass function	32
2.2.2	mRNA transcription	35
2.3	Comparison of MGM with BGM	41
2.3.1	Mean cell size	41
2.3.2	Size variability on the population level	43
2.3.3	Cell cycle timings	44
3	Discussion	46
4	Appendix	50
4.1	Model species, parameters and equations	50
4.2	Model code	54

Chapter 1

Introduction

1.1 Motivation

In 2019 Altenburg et al. proposed a model for volume growth of single yeast cells (*s.cerevisiae*) [1] (hereafter VGM). Their goal was to provide a mechanistic explanation for changes of the cell volume. The model was based on thermodynamic principles, as opposed to phenomenological descriptions of volume trajectories. It included external and internal osmolyte concentrations and could accurately reproduce cellular reactions in osmotic shock experiments. Additionally an extended version of the model was able to simulate the growth of mother cells and buds. The simulations were limited to one cell cycle and the duration of the cell cycle phases were fixed. A natural expansion of the model would be to cover several generations and to introduce an active cell cycle regulation. This would be an opportunity to test its validity on long time scales and for variable cell phase durations.

In 2012 Spießer et al. presented a model that provided a framework for cell cycle regulation [14] (hereafter BGM). It was based on auto catalytically growing cells. As these cells grew and divided over many generations a large and diverse population formed. Even though rapid advances are made in the acquisition of single cell data, a clear understanding of experimental results still is often clouded by measurements over large numbers of cells. This allows observations only on averaged mean cells and can lead to confusion of individual cell characteristics with emergent properties of the ensemble. An example is the homeostasis of cell size on the population level,

whilst single cells do not necessarily stop growing. The simulation of *in silico* ensembles can help to reproduce such experimental results and shed light on underlying mechanisms. If the VGM was to successfully replace the growth module for single cells in the BGM such *in silico* experiments could be performed for the VGM too. The inculsion of osmolyte concentrations in the VGM could be used to study the effects of osmotic shocks and variation of the osmolyte concentration of the growth medium on whole populations, instead of just single cells.

1.2 The cell cycle of yeast

Many organisms divide symmetrically. Budding yeast is unusual in that it divides asymmetrically [8]. Whilst growing it bulges out and forms a bud. After some time the bud separates from the parent cell. In this process all the necessary components, such as the DNA have to be replicated and transferred to the bud. Cells that bud for the first time are called *daughter* cells. Older cells are called *mother* cells. The cycle of growth and division is generally divided in two main phases, the interphase (I), where all growth related processes happen and the mitotic phase (M), where the parent cell and the bud separate. The interphase is again subdivided into a first gap phase between division and DNA-replication (G1) where only the parent cell grows. This is followed by a synthesis phase (S) where, after passing the start signal (START) at the end of G1, DNA-replication and bud formation begin. Then comes a second gap phase (G2) where the parent cell and bud continue growing and the duplicated nucleous is transferred to the bud.

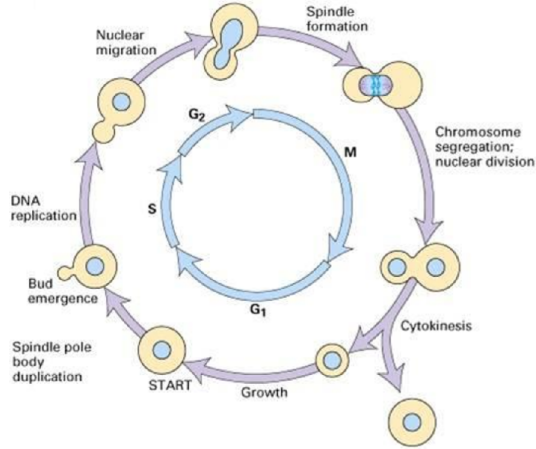


Figure 1.1: Cell cycle in yeast. Figure taken from [4]

The progression from one phase to another is controlled by a vast network of signalling proteins. It culminates in the expression of a cascade of genes at each transition [12]. Two important protein classes in this network are cyclins and cyclin-dependent-kinases (CDK). A kinase is an enzyme that attaches a phosphate group to its substrate, hence drastically changing its biochemical properties. In order to be active CDK's need a cyclin to bind to them. Depending on the binding cyclin they target different substrates [5].

Another important class of regulatory proteins is called transcription factors. They regulate the activity of genes by binding to strands of DNA. This changes its morphology and binding sites for RNA-polymerases are inhibited or promoted. The activity of many transcription factors is regulated by phosphorylation and dephosphorylation [9].

Here the cyclins come into play. When the right cyclin is abundant in sufficient amounts the CDKs target specific transcription [5] factors and the genes for transition to the next cell phase are expressed.

The following simplified description of the network regulating the transition from the G₁ phase to the S phase is based on Barber et al. 2020 [3].

During the early G₁ phase the inhibitor Whi5 is localized in the nucleus of the cell. There it binds to the transcription factor SBF and inactivates it. Active SBF induces the transcription of the genes

needed for the phase transition. The cyclin Cln3 binds to the cyclin dependent kinase Cdk1 and phosphorylates Whi5. Phosphorylated Whi5 releases SBF and is exported from the nucleus. The now free SBF induces the transcription of several other cyclins, Cln1 and Cln2 among the first. These cyclins further phosphorylate Whi5, leading to a positive feedback loop and subsequent transition to the S phase.

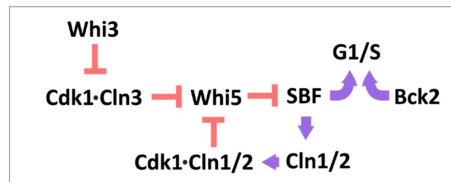


Figure 1.2: Schematic representation of the regulation of the G1 phase in yeast.
Figure taken from [3]

1.3 The biomass growth model

The BGM simulates populations of independently growing yeast cells (*s.cerevisiae*). As they go through a cycle of cell phases they grow buds and divide when the buds are mature enough. As a result the number of cells in the population increases significantly over time. The duration of the cell cycle phases are a subject of intensive study and the precise coordination of cell growth and division remains to be determined. The BGM aims at illuminating the underlying processes and proposes a possible mechanism. At its core lies a balance between the cells' capacity to synthesize *cyclins* and their rate of degradation. In this way cell cycle progression becomes a function of the metabolic capacity of the cell. Cyclins are certain proteins that are part of a vast signalling network, which controls the activity of cell phase specific genes sites and regulates the transition from one phase to the next. These phase transitions are often induced by switch like behavior of the system, when key cyclins reach a critical level. Once this threshold is overcome, the genetic program for the next phase is started.

A greatly simplified model of this regulatory machinery is implemented in the BGM. It comprises of two dummy cyclins *Cln* and *Clb* and their mRNA. The cell cycle is divided into four phases (G1,

S, G2, M), the transition from one to another is implemented as an instantaneous event. The durations of the S and M phase are fixed, while the G1 and the G2 phase end when Cln and Clb levels reach a threshold respectively. Their production is described by a second order reaction kinetic, which depends on the available mRNA and the metabolic capacity of the cell. Including a first order degradation kinetic the time derivative of the cyclin concentration $\frac{Cln}{V}$ is given as

$$\frac{d}{dt} \left(\frac{Cln}{V} \right) = k_p \cdot mCLN \cdot B_R \frac{A}{V^2} - k_d \cdot \frac{Cln}{V} - n \cdot \frac{\dot{V}}{V^2} \quad (1.1)$$

Computationally easier is the time derivative of the number of cyclin molecules Cln

$$\dot{Cln} = k_p \cdot mCLN \cdot B_R \frac{A}{V} - k_d \cdot Cln \quad (1.2)$$

k_p and k_d are the production and degradation rate constants, $mCLN$ and B_R the mRNA and the *internal* biomass, A and V the surface and volume of the cell. The term $B_R \cdot A$ represents the metabolic capacity of the cell. Spießer et al. justified its dependence on the cell surface with the availability of nutrients, as for an increasing area of the cell membrane the uptake of nutrients should increase as well [14].

The mRNA is produced in stochastic bursts, independently of the metabolic capacity. This makes the duration of the G1 and G2 phase noisy, which produces asynchronous cell cultures.

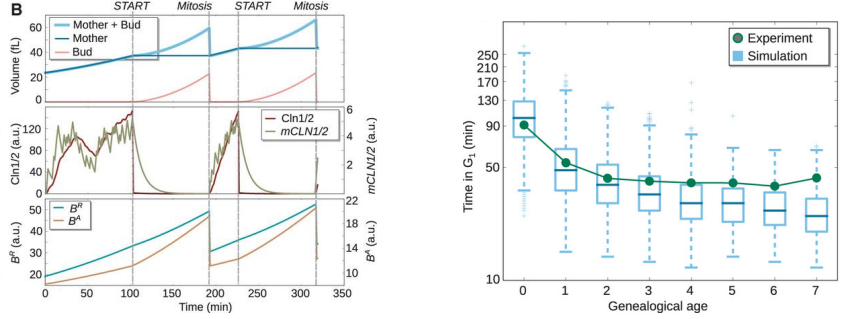
Similar to the cyclins the total cellular biomass B is produced as a function of the internal biomass and the biomass precursor mB .

$$\dot{B} = k_p \cdot mB \cdot B_R \frac{A}{V} - k_d \cdot B \quad (1.3)$$

The biomass itself is divided into biosynthetically active, *internal* biomass and inactive *structural* biomass of which the cell membrane and wall comprise. The metabolic capacity of the cell is allocated between the two according to the allocation parameters k_R and k_A :

$$\dot{B}_R = \dot{B} \cdot \frac{k_R}{k_R + k_A} \quad (1.4)$$

$$\dot{B}_A = \dot{B} \cdot \frac{k_A}{k_R + k_A} \quad (1.5)$$



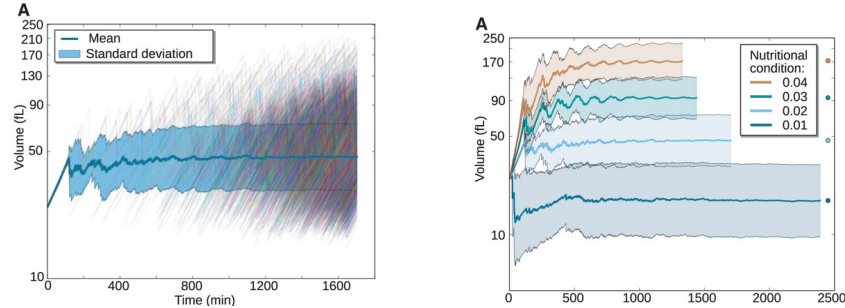
(a) Temporal evolution of mean cell volume with standard deviation. The thin lines represent single cell volume trajectories. (b) Average time spend in G1 depending on genealogical age. Comparison of experimental data and a simulated population

Figure 1.3: Figures taken from [14]

This model for biomass synthesis results in auto catalytic growth, which normally leads to exponential growth of the cell. Because in this case the rate of biosynthesis is scaled with the surface to volume ratio (eq. 1.3) cell growth is more polynomial. It is slowed down through a feedback created by the proportionality of the structural biomass to the cell surface $B_A \sim A$.

During the G1 phase the mother grows undisturbed until the amount of *Cln* reaches the necessary threshold for a cell phase transition. Upon entering the S phase the mother stops growing and a bud begins to form. Fig. 1.3a shows the trajectories of a single cell over two generations. One can see the Volume of mother and bud, the amount of *Cln1/2* and its mRNA and the internal and structural biomass. After the mitosis the mother and the bud separate and split up the internal biomass and remaining cyclins between them. In accordance with experimental observations the BGM predicted a distinct drop of the average G1 phase duration between the very first generation (daughter cells) and the second generation (mother cells).

On the population level the mean cell size converged to a stable value (fig. 1.4). The BGM allows the tuning of the cellular growth rate. As is observed in experiments (fig. 1.4), the mean cell size is a function of this rate.



(a) Temporal evolution of mean cell volume (b) Mean cell size and standard deviation with standard deviation. The thin lines for cultures simulated for different growth rates.

Figure 1.4: Figures taken from [14]

1.4 The volume growth model

The VGM describes the volume trajectories of single cells. While the BGM looks at growth from a metabolic angle namely the cells capacity to produce new biomass, the VGM aims at a mechanistic explanation for cell growth. The core idea is that pressure differences between the inside and the outside of the cell result in a water flux J_w across the cell membrane. Two kinds of pressure are considered to act on the cell, osmotic pressures and mechanic pressure. The osmotic pressures depend on the concentration of osmolytes inside and outside of the cell (c_i and c_e) and are hence called internal and external osmotic pressure (Π_i and Π_e). They are calculated using the equation for an ideal gas as

$$\Pi_i = c_i \cdot R \cdot T \quad (1.6)$$

$$\Pi_e = c_e \cdot R \cdot T \quad (1.7)$$

with the gas constant R and the temperature T . The mechanic pressure stems from the elastic deformation of the cell wall due to water influx. Like when filling a balloon with water a counter pressure builds up, which is called the turgor pressure Π_t . In a simplified view the volume of a cell is split into space taken up by solid macromolecules, e.g. osmotically *inactive* volume and water with all soluble components, e.g. osmotically *active* volume. The osmotically active volume V_{os} changes according to the water flux J_w .

Written for the radius r of a spherical cell:

$$\dot{r}_{os} = -J_w \quad (1.8)$$

Based on a formalism established by Kedem-Katchalsky [10] J_w can be described as the difference between the osmotic pressure gradient across the cell membrane and the tugor pressure of the cell wall

$$J_w = -L_p (\Pi_t + \Pi_e - \Pi_i) \quad (1.9)$$

where L_p is the hydrolic conductivity of the membrane. Both tugor pressure and internal osmotic pressure are sensitive to the cell volume and its time derivative. This creates a feedback loop on the water flux and the cell growth. A quasi steady state of the pressure gradient and cell growth establishes.

The internal osmolyte concentration changes due to osmolyte uptake, consumption and dilution. Uptake and consumption are dependent on the cell surface and volume respectively and dilution on both, the cell volume and its derivative. Written for the cell radius r it reads

$$\dot{c}_i = 3 \frac{k_{up}}{r} - k_{cons} - 3 \frac{c}{r} \dot{r} \quad (1.10)$$

Changes of the cell volume cause elastic and plastic of deformation of the cell wall. While elastic deformation increases the tugor pressure, plastic deformation releases it. It is associated with the incorporation of new cell wall materials. The two types of deformation are described by a Hookean and a Bingham-Norten element connected in series. Assuming that the radius r of the cell is much greater than the thickness d of the cell wall the dynamics of the tugor pressure can be described by the following equation

$$\dot{\Pi}_t = \frac{2Ed}{1-\nu} \frac{\dot{r}}{r^2} - \Pi_t \frac{\dot{r}}{r} - \frac{E\Phi}{1-\nu} f_m(\Pi_t, \Pi_{ct}) \quad (1.11)$$

where f_m is only zero for tugor pressures above the critical pressure for plastic deformation Π_{ct} .

The model predicts a maximum cell radius, which depends on the osmolyte uptake and consumption rate constants in eq. 1.10

$$r_{max} = 3 \cdot \frac{k_{up}}{k_{cons}} \quad (1.12)$$

Fig. 1.5 shows the volume trajectories for different ratios of osmolyte uptake and consumption rate.

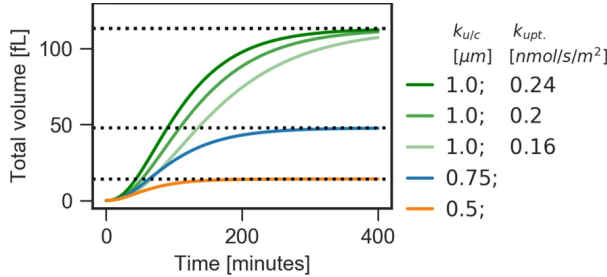


Figure 1.5: Temporal evolution of cell volume. The ratio between k_{uptake} and $k_{consume}$ determines the maximum cell volume. If this ratio is kept constant but k_{uptake} and $k_{consume}$ increased or decreased only the effective growth rate changes. Figure taken from [1]

During their life span *S.cerevisiae* cells do not only grow, but divide and birth new cells all the time. They undergoes an unequal division with a big mother and a small new born daughter cell, where the daughter cell first develops as a bud on the mother, before they split when she is mature enough. The VGM models the growth of the bud by first simulating the mother for a time t_{start} . Then a second, very small cell is spawned, representing the bud. Both cells are connected through a bud neck, allowing the exchange of water and osmolytes between them. The water exchange is driven by their turgor pressure gradient, the osmolyte exchange by their osmolyte concentration gradient.

$$J_w = \dots + k_{diff}^w \cdot (\Pi_t^m - \Pi_t^b) \quad (1.13)$$

$$\dot{c}_i = \dots + k_{diff}^c \cdot (c_i^m - c_i^b) \quad (1.14)$$

A complex balance develops between them. A feature which will get greater attention later on was the different cell wall extensibility Φ of the mother and the bud. Fig. 1.6 shows their volume trajectories for different ratios q and a schematic representation of their coupling.

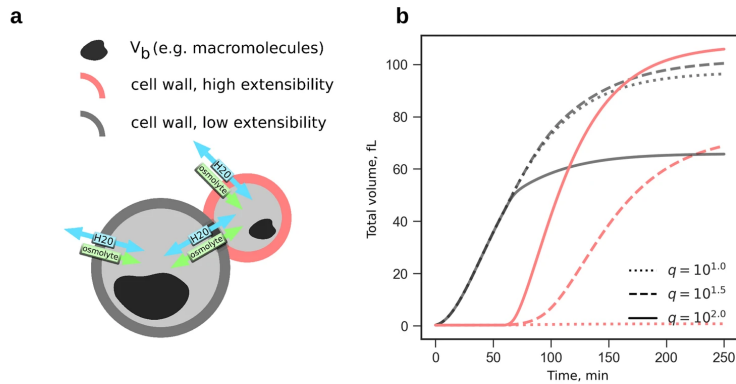


Figure 1.6: Figure take from [1]. (Left) Scheme of mother/bud coupling. (Right) Growth trajectories of mother and bud for different ratios of their cell wall extensibilities. Figure taken from [1]

Chapter 2

The merged model

The following chapter presents the results of combining both models, the BGM and the VGM, into a merged model. In this process the models had to be extended and adjusted in parts to meet each other. Notably the VGM had to be expanded to cover multiple generations. The problems and the proposed approaches to solve them are described in the first section. The second section aims at integrating the cyclin based cell cycle regulation of the BGM into the now expanded VGM. The last section compares key simulation results of the merged model with the BGM.

2.1 Expanding the VGM to multiple generations

The VGM is primarily designed for the simulation of one cell cycle. In order to integrate it into the a population framework it has to be expanded to cover multiple generations. A key difficulty is the process of cell division, when the mother cell and the bud are coupled and water and osmolytes are exchanged between them. *Coupled implementations* describes these issues first for the basic model as presented by Altenburg et al. 2019 [1] and second for two alternative implementations. This evaluation then leads to the simpler model used for the merged model, presented in *decoupled implementation*.

2.1.1 Coupled implementations

Analysis of the basic model

The model works fine, as long as only one period of the cell cycle is considered. Difficulties arise, when simulating several generations. Upon each division the coupled cells have to be decoupled. The terms for water and osmolytes exchange between them are removed and both continue the simulation as separate systems. This disturbs their balance. The effects vary on the chosen parameters and the precise implementation of the model. Figure 2.1 shows three plots of a cell simulated over several generations with buds emerging in fixed intervals. At the top the radius of the mother (blue) and the buds (cyan) is plotted over time, in the middle the concentration of osmolytes and at the bottom the turgor pressure.

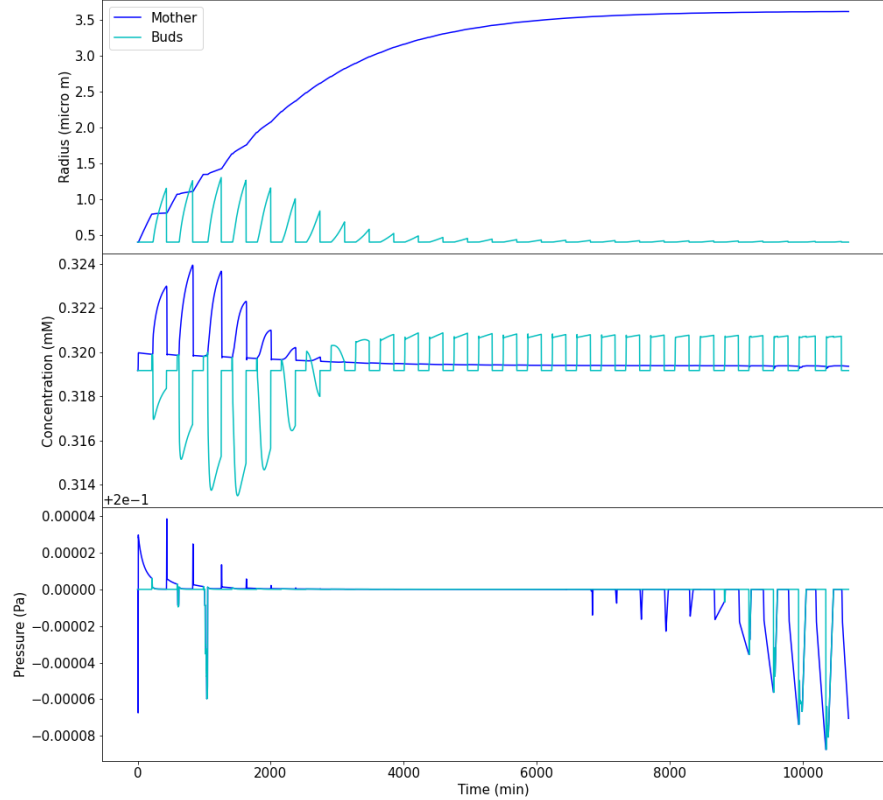


Figure 2.1: Temporal evolution of cell radius, osmolyte concentration and turgor pressure of a mother (blue) and buds (cyan). Simulated with a simple implementation of the VGM expanded to several generations.

It is a good example, as it illustrates typical behaviors of the system. The graphs can be divided into three phases. In the first phase the osmolyte concentration and the turgor pressure of the bud are higher than that of the mother (budded periods). During this time the buds grow at the expense of the mother, since water and osmolytes follow the gradient towards the buds. This is in line with the experimental observation that the mother barely grows during the budded phase [8]. It should be noted though that in this simulation the effect is

strongest in the first few generations. There the mother is yet very small and the final size of the buds even surpasses that of the mother. This is not in accordance with experimental data. It is well established that *S.cerevisiae* undergoes an unequal division and buds at birth are basically always smaller than mother cells [8]. Another observation from figure 2.1 is that already after three generations the birth size of the buds becomes smaller. After seven generations the concentration of osmolytes and the turgor pressure of the mother become lower than that of the buds and the next phase starts. The flow of water and osmolytes between mother and bud gets reversed. Now the mother grows on the expense of the buds. They no longer really grow and stay at their initial volume. This phase continues until the mother approaches its maximum cell radius, which is given by the ratio of her osmolyte uptake and consumption rate [1].

$$r_{max} = 3 \cdot \frac{k_{uptake}}{k_{consumption}} \quad (2.1)$$

At some point the growth boosts of the buds help the mother to overcome this limit during the budded period. The last phase begins. It is best recognizable for the dropping turgor pressure after cell divisions in the last generations.

Before presenting approaches to 'fix' the impaired bud growth comes some more in-depth analysis of the system. Two primary questions request further attention:

1. Why are the osmolyte concentration and the turgor pressure of the mother higher than that of the bud during the first phase of the simulation? Should it not be the other way around?
2. Why does the turgor pressure of the mother fall after every cell division during the last phase of the simulation?

In an 'undisturbed' simulation (without budding) the general trend for the osmolyte concentration and the turgor pressure of the cell is to fall towards a limit point. Therefor, if the cell parameters are the same for both, when the bud is spawned it should have a higher osmolyte concentration and turgor pressure than the mother (Figure 2.2 left). In a coupled simulation osmolytes and water should then flow towards the mother. Depending on the gradients between them, this may result in the bud not growing at all, as in figure 2.2 (right).

So the first question could be reformulated to be: Why does the bud grow in the first place?

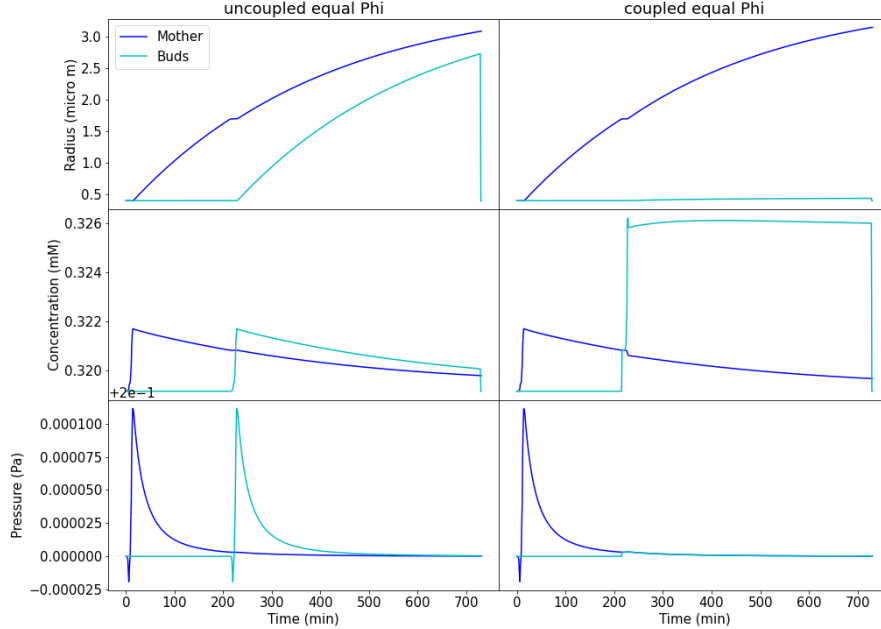


Figure 2.2: Temporal evolution of cell radius, osmolyte concentration and turgor pressure of a mother (blue) and buds (cyan) over one cell cycle. Equal cell wall extensibility for mother and bud, coupled and decoupled implementation.

The answer is that in their implementation of a coupled growth (on which the results in figure 2.1 are based) Altenburg et al. did not chose the same cell parameters for mothers and buds [1]. They described that for buds to grow in their model, either the cell wall extensibility Φ needed to be at least ten to a hundred times higher than that of the mother, or the Young's modulus E needed to be considerably lower than that of the mother. The idea was fueled by studies that showed a delayed incorporation of chitin into the buds' cell wall, hence changing its mechanical properties. A significantly lower Young's modulus of the bud was rejected after measurements of the cell wall stiffness via atomic force microscopy. On the contrary they found that the Young's modulus of buds was increased by a

factor of 1.3 compared to the mother. This left only the cell wall extensibility as the deciding factor to allow bud growth.

A high cell wall extensibility immediately reduces the buds' turgor pressure, as a comparison of the left sides of figure 2.3 and figure 2.3 demonstrates. The simulations are the same in both figures, only the cell wall extensibility is now higher in the bud than in the mother. By adjusting this parameter the turgor pressure of the bud can be tuned to be lower than that of the mother. Consequently the pressure gradient is advantageous for the bud and in a coupled simulation water flows from the mother to the bud, allowing bud growth (figure 2.3, right).

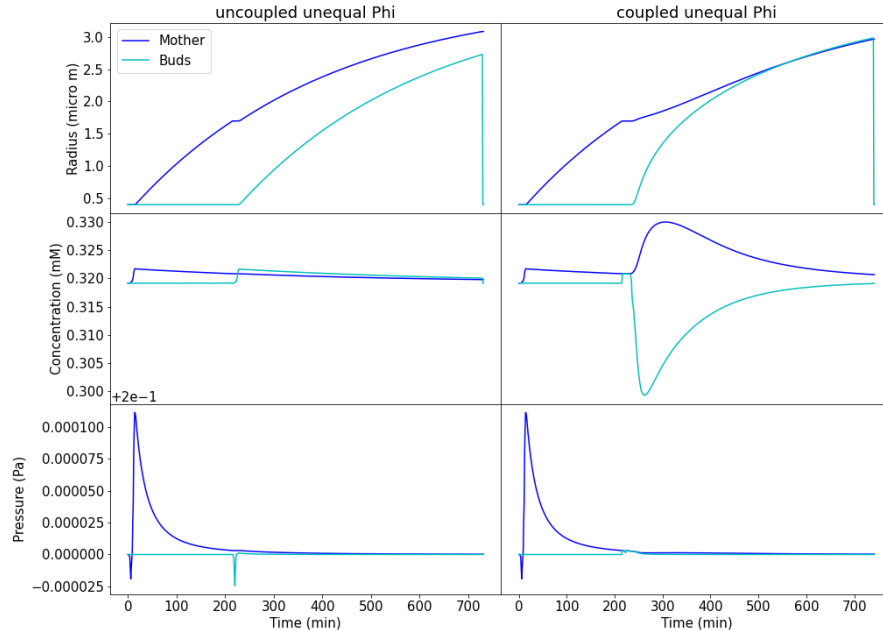


Figure 2.3: Temporal evolution of cell radius, osmolyte concentration and turgor pressure of a mother (blue) and buds (cyan) over one cell cycle. Unequal cell wall extensibility for mother and bud, coupled and decoupled implementation.

An analysis of the model equations helps to better understand this phenomenon. Equation 1.11 shows the time derivative of the turgor pressure Π_t as a function of itself, the cell radius r and its'

time derivative \dot{r} (reprinted here).

$$\dot{\Pi}_t = \frac{2Ed}{1-\nu r^2} \frac{\dot{r}}{r} - \Pi_t \frac{\dot{r}}{r} - \frac{E\Phi}{1-\nu} f_m(\Pi_t, \Pi_{ct})$$

The first two terms on the right hand side capture the effect of *elastic* deformation of the cell wall. As will be explained in a later section, under normal conditions their sum yields an increasing turgor pressure for an increasing cell radius. The third term represents the effect of *plastic* deformation of the cell wall. The factor $f_m(\Pi_t, \Pi_{ct})$ is non zero when $\Pi_t > \Pi_{ct}$. This means that the last term is only active, when the turgor pressure of the cell rises above the critical threshold value Π_{ct} . It then plays an antagonistic role to the other terms and *reduces* the turgor pressure. The cell wall extensibility Φ determines the strength of this response. When it is increased, the systems reaction is stronger and consequently the turgor pressure decreases.

The first half of question number one, which was concerned with the turgor pressure, is answered. The second half, which looked at the osmolyte concentration and why it is higher for the mother than the bud (figure 2.1), is yet to be answered. An explanation can be found in the equation 1.10 describing \dot{c}_i the change of the osmolyte concentration over time (reprinted here):

$$\dot{c}_i = 3 \frac{k_{up}}{r} - k_{cons} - 3 \frac{c}{r} \dot{r}$$

A term of particular interest is the dilution term $-\frac{c}{r}\dot{r}$. Changes of \dot{r} directly affect it. The faster the cell grows, the faster the osmolyte concentration is diluted. The same is true in reverse. When mother and bud are coupled water is exchanged between them. The exchange is driven by their different turgor pressure. If the cell wall extensibility of the buds is set much higher than the mothers', the pressure gradient between them turns in favor of the bud, as was described earlier. This means the buds' radius grows faster and consequently its osmolyte concentration is diluted stronger. At the same time the mother grows slower and its osmolyte concentration is diluted less. This turns the osmolyte gradient in favor of the bud too and causes an osmolyte flow from the mother to the bud (figure 2.3 right).

The same phenomenon in reverse occurred in the simulation with

equal Φ for mother and bud in figure 2.2. The turgor pressure of the bud is not reduced compared to the mother and the gradient between them is in favor of the mother. Water flows from the bud to the mother, diluting its osmolyte concentration. Consequently the gradient becomes shifted even more in favor of the mother. Figure 2.2 shows this, when upon initialization of the bud, the osmolyte concentration of the mother suddenly drops and that of the bud is much higher than in the uncoupled simulation.

The second question was: 'Why does the turgor pressure of the mother fall after every cell division during the last phase of the simulation?'. The answer has two parts. First the turgor pressure is falling, when the cell radius is shrinking and below the threshold in inequality 2.2. Second when the mother approaches her maximum cell radius defined in equation 2.1 she shrinks after cell divisions and grows while coupled with a bud. Hence the turgor pressure falls during the unbudded periods.

To prove the first statement equation 1.11 is analyzed again:

$$\dot{\Pi}_t = \frac{2Ed}{1-\nu} \frac{\dot{r}}{r^2} - \Pi_t \frac{\dot{r}}{r} - \frac{E\Phi}{1-\nu} f_m(\Pi_t, \Pi_{ct})$$

As explained earlier the right hand side can be divided into changes of turgor pressure due to *elastic* or *plastic* deformation. The term for plastic deformation is always either zero or negative and therefore not of further interest. If the turgor pressure is decreasing below the critical threshold value Π_{ct} , its derivative is negative, when the sum of the two terms for elastic deformation are smaller than zero.

$$\frac{2Ed}{1-\nu} \frac{\dot{r}}{r^2} - \Pi_t \frac{\dot{r}}{r} < 0$$

This can be reformulated as a condition on the cell radius. If the radius is decreasing ($\dot{r} < 0$) it reads as follows:

$$\frac{2Ed}{1-\nu} \frac{1}{\Pi_t} > r \quad (2.2)$$

As long as the radius is below that value, the derivative of the turgor pressure is negative, when the cell becomes smaller. This is always true in the simulations depicted here. An interesting case occurs, when the rates for osmolyte uptake and consumption are chosen in

such a way, that the maximum cell radius (equation 2.1) is higher than the left hand side of inequality 2.2:

$$\frac{2Ed}{1-\nu} \frac{1}{\Pi_t} < 3 \cdot \frac{k_{up}}{k_{cons}}$$

Then the cell radius can grow above this threshold value and the derivative of the tugor pressure becomes negative, even though the cell radius is still increasing. This would result in even faster growth, as equation 1.9 shows:

$$J_w = -L_p (\Pi_t + RTc_e - RTc_i)$$

The water influx is dependent on the tugor pressure Π_t , the *internal* osmolyte concentration c_i and the *external* osmolyte concentration c_e . The latter is constant, making J_w dependent only on the difference $\Pi_t - RTc_i$. When Π_t becomes smaller, J_w becomes bigger. But according to earlier results the osmolyte concentration decreases due to stronger dilution, when \dot{r} increases. In a feedback via equation 1.9 this reduces the influx of water and negates the growth gain. In this way the falling tugor pressure is translated directly into a falling osmolyte concentration and the cell radius grows as usually. To prove the second statement a few more steps are needed. In the last phase of the simulation the gradients of tugor pressure and osmolyte concentration work in the favor of the mother (figure 2.1). During the budded phase the mother is able to grow above the limit she could reach alone. Therefor at the time of cell division her cell radius is bigger than the maximum defined in equation 2.1:

$$r > 3 \frac{k_{up}}{k_{cons}} \quad (2.3)$$

As will be shown next, this means that her osmolyte concentration and consequently her radius must fall, until the cell radius is no longer bigger than $3 \frac{k_{up}}{k_{cons}}$. As a recapitulation, the equation for the osmolyte concentration (equation 1.10) is:

$$\dot{c}_i = 3 \frac{k_{up}}{r} - k_{cons} - 3 \frac{c}{r} \dot{r}$$

When the derivative of c_i is negative, the right hand side of equation 1.10 must be smaller than zero. This defines a condition on the cell radius:

$$r > 3 \frac{k_{up}}{k_{cons}} - 3 \frac{c}{k_{cons}} \dot{r} \quad (2.4)$$

The faster the cell grows, the lower the threshold is. It should be noted that under normal, undisturbed growth conditions the cell radius is always above this value, which is why the osmolyte concentration generally falls. When in a late stage of a coupled simulation the bud separates from the mother, she loses the growth boosts from the bud and stops growing. The condition 2.4 is simplified and becomes similar to the definition of the maximum cell radius:

$$r > 3 \frac{k_{up}}{k_{cons}}$$

As stated in inequality 2.3 this is satisfied and consequently the mothers' osmolyte concentration falls. This has a negative effects on the cells' water uptake (equation 1.9) and the cell shrinks ($\dot{r} < 0$). To come back to the answer of the original question: After the cell division the osmolyte concentration of the mother falls. This causes a negative derivative of the cell radius, which in the end results in a falling turgor pressure.

Alternative implementations

In the next section two alternative approaches to implement the multi generational VGM are presented. They are different to the version described above in either:

1. having an adaptable budded phase duration
2. or the cell wall extensibility Φ of the mother being reduced with every generation

The first variation is motivated by key results of Spießer et al. [13]. They suggested an adaptive duration of the G2 phase and linked its regulation to the metabolic capacity of the bud. This ensured sufficient maturity of the buds at cell division. A simple way to implement this idea into the VGM is to define a critical bud size. When it is reached the signal for separation is given and the budded phase ends. Hence a sufficient size of the buds is guaranteed in every generation.

The other variation is based upon the observation, that during their lifetime the cell wall of budding yeasts gets increasingly scarred. These so called 'bud scars' stem from former cell divisions, where the process of separation left marks on their surface. After generations of budding the cell wall becomes more and more rigid and less

able to expand. In the language of the VGM this phenomenon can be captured by reducing the mothers' cell wall extensibility Φ after every cell cycle. Already earlier this was used in reverse (increased Φ of the buds), to make bud growth possible even over just one cell cycle. The cell wall extensibility influences the turgor pressure and a high Φ of the mother changes the pressure gradient in favor of the bud. This way bud growth can be enhanced and sustained even in later generations.

A natural third variation is the combination of both approaches. Figure 2.4 shows the simulation results of all three implementations as well as the standard version. Again the plots at the top show the temporal evolution of the cell radius, the plots in the middle that of the osmolyte concentration and those at the bottom the turgor pressure. The standard implementation and that with bud scars both have a fixed duration of the budded phase and the size of the buds decreases with every generation. Nevertheless there is a clear benefit on bud growth for the version with bud scars. As expected the other two versions, the one with an adaptive duration of the budded phase and the combined one, produce buds of constant birth size. This comes at the cost of increasingly long budded phases. Here too introduction of bud scars facilitates faster bud growth and consequently shorter generation times. Nevertheless as the mother cell approaches her maximum radius, the budded phases become intolerably long. Additionally while these model adjustments seemingly resolve the issue of bud growth, it is a cosmetic 'bug fix' that can not be backed up by experimental data. On the contrary the duration of the budded phase seems to slightly decrease with genealogical age [7].

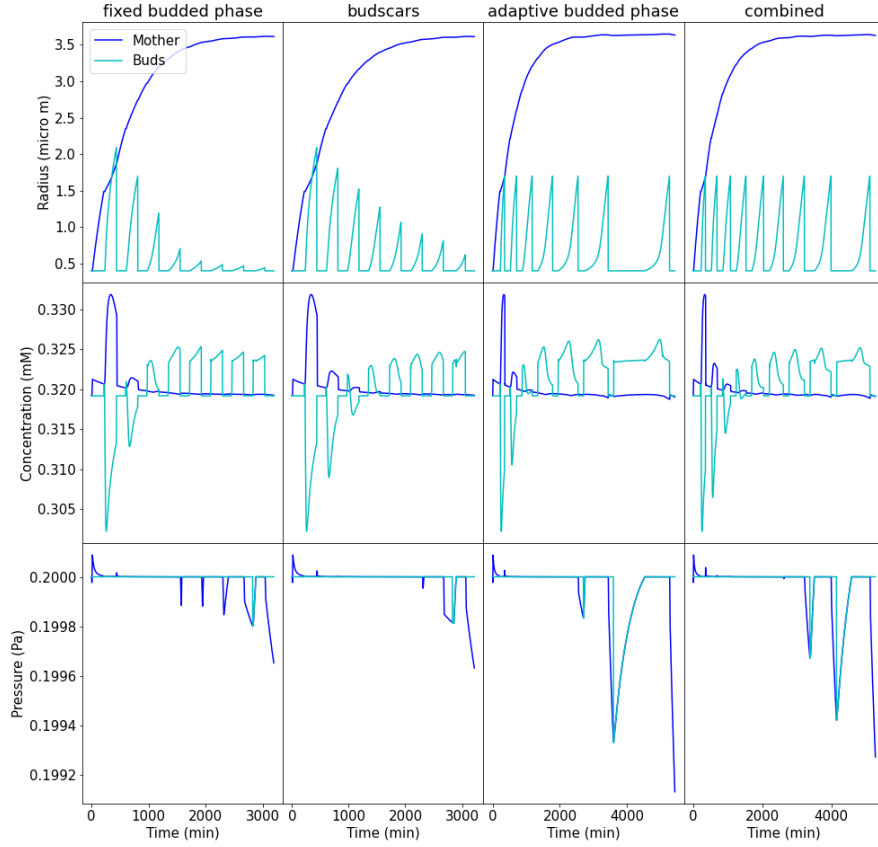


Figure 2.4: Temporal evolution of cell radius (top), osmolyte concentration (middle) and turgor pressure (bottom) of a mother (blue) and buds (cyan). Comparison of four different model implementations, from left to right: a fixed duration of budded phase; a fixed duration of budded phase, with mother acquiring bud scars over the generations; an adaptive duration of budded phase, but no bud scars; an adaptive duration of budded phase and bud scars.

2.1.2 Decoupled implementation

In light of these difficulties a simpler approach has been chosen. Instead of coupling mother and bud they are both treated as independently growing cells. Figure 2.5 shows simulation results of this

new model version. During the unbudded phase of the cell cycle only the mother grows. Then a bud is initialized. During this phase only the bud grows. The mother pauses and resumes growth after the cell division.

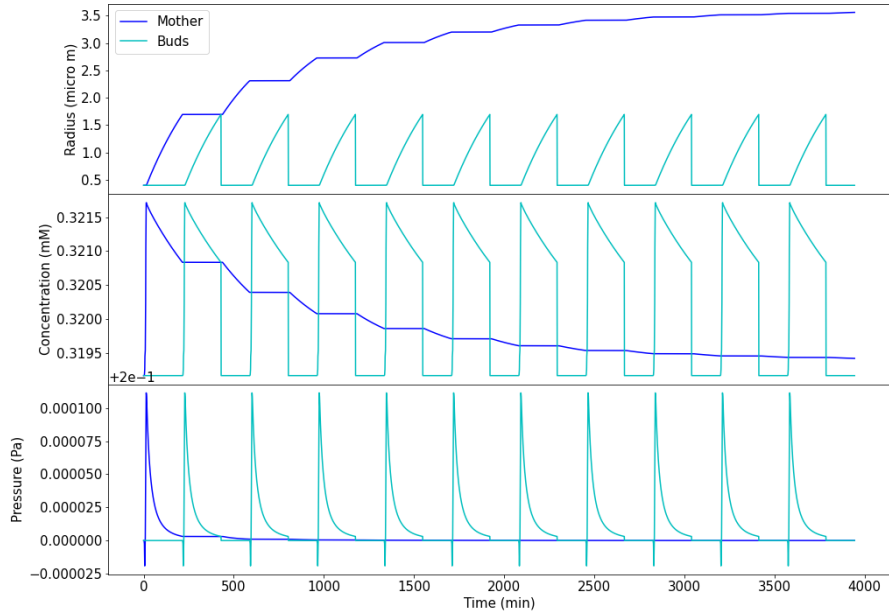


Figure 2.5: Temporal evolution of cell radius (top), osmolyte concentration (middle) and tugor pressure (bottom) of a mother (blue) and buds (cyan). Simulated with decoupled implementation of VGM.

This forced growth break instead of a ‘naturally’ damped growth of the mother is more simplistic than a coupled model. Nevertheless it has a paragon in the BGM. There the production of cell volume (‘structural biomass’) is redirected entirely from the mother to the bud during the budded phase. This switch is induced by an ‘artificial’ parameter change at the transition from the G1 to the S phase. An important difference of an uncoupled implementation of the VGM to the BGM though is the influence of the mother on the buds’ growth. Within the BGM the growth of the cell volume is

dependent on the metabolic capacity of the cell. Since this capacity to 'produce' volume increases with the size of the cell, the buds grow faster for older mothers. In a decoupled implementation of the VGM the status of the mother has no influence on the growth of the bud. This is probably unrealistic, but as explained earlier, while a coupled implementation provides an influence of the mother on the buds' growth, this influence is not necessarily a realistic one either. The main objective of this thesis is to integrate the basic single cell growth model of the VGM into a population framework and to introduce the cyclin network of the BGM into its cell cycle regulation. For this reason the choice here is for simplicity.

2.2 Cell cycle regulation

The duration of the cell cycle and the time t_{start} from cell division until a new bud begins to form is individual for every cell. Altenburg et al. fitted the VGM to volume trajectories of mothers and their bud, measured over one generation [1]. Although they could reproduce the experimental data, using t_{start} as an input, the model did not provide a mechanism for t_{start} to emerge as an output.

The BGM on the other hand is build around such a mechanism. It links the regulation of the cell cycle with the metabolic capacity of the cells and can be applied to the VGM. Eq. 1.2 described the dynamics of the cyclin molecule numbers as

$$\dot{Cln} = k_p \cdot mCLN \cdot B_R \frac{A}{V} - k_d \cdot Cln$$

To apply this equation to the VGM an adjustment is necessary. In contrast to the BGM the VGM explicitly computes the osmolyte concentration, which varies little over time. Since most nutrients act as osmolytes, a bigger cell surface does consequently not increase nutrient availability in the VGM. The scaling of cyclin production with the cell surface would create a false increase of the cells' metabolic capacity and has to be removed. The resulting equation for Cln is

$$\dot{Cln} = k_p \cdot mCLN \cdot \frac{B_R}{V} - k_d \cdot Cln \quad (2.5)$$

The production of the two cyclins Cln and Clb is dependent on the metabolic (internal) biomass B_R and the mRNA concentration

$\frac{mCLN}{V}$. In the following two sections both quantities are redefined in the context of the merged model.

2.2.1 Biomass function

The VGM provides only a rudimentary biomass, the osmotically inactive volume V_b . It is proportional to the volume of the relaxed cell V_{ref} . This has implications for the density of the cell as measured by the biomass divided by the total cell volume $\frac{B}{V}$. The trajectories of the total cell volume and the relaxed cell volume are not fully aligned and their ratio changes over time. Consequently the density of the growing cell changes significantly. However experimental studies suggest that the cell density of *s.cerevisiae* is more or less constant, apart from periodic variations of about 1 % during the cell cycle [2]. Therefor the original assumption of the cells' biomass being proportional to the relaxed cell volume will be slightly altered to it being proportional to the total cell volume. For a given cell density ρ_{cell} the biomass of a cell is

$$B = \rho_{cell} \cdot V \quad (2.6)$$

It comprises of all macro molecules present in the cell from proteins to lipids to DNA, of which by far not all are metabolically active. Nonetheless following the example of the BGM the biomass is divided in two kinds

- structural biomass B_A
- metabolic biomass B_R

The structural biomass represents the cell wall, the cell membrane and its various proteins. The metabolic biomass is all the rest. It will be used in the equations for cyclin and mRNA production. Together they add up to the total biomass

$$B = B_A + B_R \quad (2.7)$$

Cell volume

The VGM differentiates between the osmotically active volume V_{os} , which changes according to water in- and out flux, and the osmotically inactive volume V_b , which corresponds to the volume that the

dried up biomass would occupy. Both volumina contribute to the total cell volume

$$V = V_{os} + V_b \quad (2.8)$$

It is useful to define a dry biomass density ρ_b as the ratio of the biomass and the osmotically inactive volume

$$\rho_b = \frac{B}{V_b} \quad (2.9)$$

With this definition the cell volume can be expressed as a function of the osmotically active volume, instead of depending on both V_{os} and V_b . Eq. 2.8 rewrites to

$$V = V_{os} + \frac{B}{\rho_b}$$

Since the biomass is proportional to the cell volume (eq. 2.6) the equation becomes

$$V = V_{os} + \frac{\rho_{cell}}{\rho_b} \cdot V$$

and the final equation is

$$V = \frac{\rho_b}{\rho_b - \rho_{cell}} \cdot V_{os} \quad (2.10)$$

For a spherical cell the radius r can be written as

$$r = \left(\frac{3}{4 \cdot \pi} \cdot \frac{\rho_b}{\rho_b - \rho_{cell}} \cdot V_{os} \right)^{\frac{1}{3}} \quad (2.11)$$

From eq. 2.10 V_b can be defined as a function of V_{os} by combining eq. 2.8 and eq. 2.10:

$$V_b = V_{os} \cdot \frac{\rho_{cell}}{\rho_b - \rho_{cell}} \quad (2.12)$$

Total biomass

For the biomass as defined in eq. 2.6 the new found eq. 2.10 leads directly to an expression of B as a function of V_{os} .

$$B = \frac{\rho_{cell} \cdot \rho_b}{\rho_b - \rho_{cell}} \cdot V_{os} \quad (2.13)$$

Structural biomass

The VGM differentiates between elastic expansion and plastic expansion of the cell wall. Only the latter is equated with 'real' growth of the cell wall and the incorporation of new structural biomass. It is monitored through the reference volume V_{ref} . The structural biomass is therefore proportional to the relaxed cell surface A_{ref} :

$$B_A = \sigma_A \cdot A_{ref}$$

where σ_A is the area density of the cell wall. Assuming all biomass has the same dry density ρ_b σ_A can be rewritten:

$$\sigma_A = \rho_b * d \quad (2.14)$$

with the cell wall thickness d . Consequently the structural biomass is

$$B_A = \rho_b \cdot d \cdot A_{ref} \quad (2.15)$$

Metabolic biomass

When the total biomass B and the structural biomass B_A is known, the metabolic biomass can be calculated according to eq. 2.7:

$$B_R = B - B_A$$

Eq. 2.13 and eq. 2.15) define B and B_A as functions of the osmotically active volume V_{os} and the relaxed cell surface A_{ref} . This allows to express B_R as a function of these quantities:

$$B_R = \frac{\rho_{cell} \cdot \rho_b}{\rho_b - \rho_{cell}} \cdot V_{os} - \rho_b \cdot d \cdot A_{ref} \quad (2.16)$$

Comparison with BGM

Defining the total biomass of the cell as a function of the cell volume differs considerably from the BGM, where *internal* (metabolic) and *structural* biomass were interdependent quantities. The rate of the biomass synthesis \dot{B} was determined by the product of the internal biomass B_R times the cell surface to volume ratio

$$\dot{B} \sim B_R \cdot \frac{A}{V}$$

The cell surface was equal to the structural biomass $A = B_A$ and for a spherical cell with $V = A^{\frac{3}{2}}$ the relation could be expressed as

$$\dot{B} \sim B_R \cdot B_A^{-\frac{1}{2}}$$

For the cellular density to be constant the ratio of the biomass and the volume must be constant

$$\frac{B}{V} = C$$

It follows that the total biomass could be expressed as a function of the structural biomass

$$B = C \cdot B_A^{\frac{3}{2}} \quad (2.17)$$

At the same time the derivative of their ratio should be zero and using the equations and relations above it follows that

$$B = \frac{2}{3} \cdot B_A \quad (2.18)$$

The two conditions in eq. 2.17 and eq. 2.18 can only be satisfied simultaneously, if the structural biomass is constant:

$$B_A = \left(\frac{2}{3} \frac{1}{C} \right)^{\frac{1}{2}} \quad (2.19)$$

This is not true for a growing cell and consequently the cellular density must change over time. It is a fundamental difference between the BGM and the adaptation of the VGM described in this thesis. A similar relation for the concentration of the internal biomass B_R/V will limit the applicability of the results in the next section to the BGM.

2.2.2 mRNA transcription

Eq. 2.5 in the opening paragraph of *cyclin expression* states, that the production rate of cyclins is dependent on the metabolic biomass and the available mRNA. In the last section the equations for the biomass as a function of the cell volume have already been established. In this section the equations for mRNA production will be defined, partially based on their implementation in the BGM.

The BGM assumed a continuous first order degradation kinetic and

stochastic bursts of transcription. For every time step of the simulation there was a certain chance for a new molecule to be added. Consequently the amount of mRNA fluctuated around an average level, depending on the transcription probability P_x and the rate constant for degradation k_d . While representing a common approach to model stochastic transcription, recent studies pointed out that such cell size independent transcription would lead to a dilution of the transcriptome in growing cells [11] and emphasized the scaling of transcription rates with cell size [15]. Consequently since translation rates for the synthesis of proteins are depended on the mRNA concentration the proteome too would be diluted. Lin et al. [11] argued, that RNA-polymerases are the rate limiting factor for mRNA transcription, similar to limitations on protein translation set by ribosomes. In both cases an excess of mRNAs/ genes sites compete for a comparatively small number of ribosomes/ polymerases. It is from this angle that eq. 1.1 must be understood, where the synthesis rate of proteins is proportional to the available internal/metabolic biomass B_R . It effectively means, that the number of translated proteins per molecule of mRNA increases with the number of ribosomes. The same logic could, and Lin et al. say should, apply to gene transcription. In the framework of the BGM this translates into scaling the transcription of mRNA with the internal biomass B_R too. Approaches on how to implement this are discussed later. Prior to that an analysis of the BGM shows, that the concentration of cyclins is indeed diluted over time. This has implications for the implementation of the cyclin thresholds. At the moment they are defined as a critical number of cyclin molecules, necessary to trigger the transition from one cell phase to the next. In a cellular context signalling networks are often sensitive to changes in concentrations. An amount based trigger would demand a special mechanism, as for example a localization of the cyclin network in a compartment of fixed volume. As for yeast the network is mainly located in the cytoplasm and the nucleous, both compartments growing with the cell size at a fixed ratio [6]. Were these thresholds implemented as concentrations, a dilution of the cyclin concentration should prolong the duration of the cell cycle with every generation and ultimately stop its progression.

Model analysis: dilution in the BGM

In their presentation of the BGM Spießer et al. focused on molecule numbers instead of concentrations [14]. They touched the topic briefly in an analysis of the causes for the homeostasis their model predicted for the average cell size in simulated populations. To test whether the implementation of the Cln-threshold as a critical molecule number had an important influence on this, they adjusted the threshold to be concentration based. The observed size homeostasis remained and the issue was dismissed. As fig. 2.6 shows, a more thorough analysis would have shown, that whilst size homeostasis on the population level could be maintained, other aspects of the model did no longer work properly. The thin lines represent single cell trajectories. Cell divisions are marked by a sharp drop in volume. While the average cell size converges as expected the individual cells become unusually large and stop dividing.

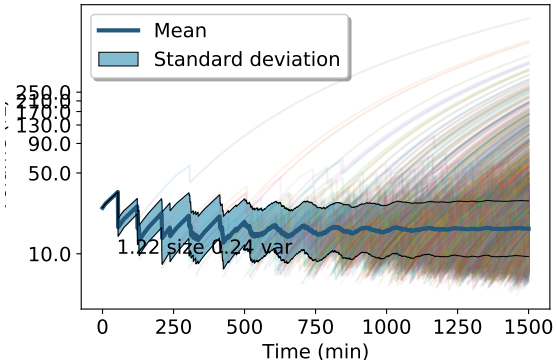


Figure 2.6: Population simulated with concentration based G1 threshold (C_{ln}). Mean volume and standard deviation plotted. Thin lines belong to single cells. Note that older cells stop budding.

Fig. 2.7 (Left) shows that the volume independent transcription of mRNA results in a dilution of the cyclin concentration, as outlined in the introduction of this section. Here the threshold is set too high to be reached and the cell is stuck in the G1 phase. When the threshold is set low enough the cell is able to reach it and progresses through the cell cycle (fig. 2.7 (Right)). After a few generations the cell stops budding. Since the cyclin concentration is steadily declining the threshold for G1 to S phase transition is

no longer met and the cell continues growing without division. This observation is underlined by the increasing duration of the G1 phase duration, shown in fig. 2.8. This clearly contradicts experimental results, which established a falling duration of the G1 phase over time, especially during the first few cell cycles [7].

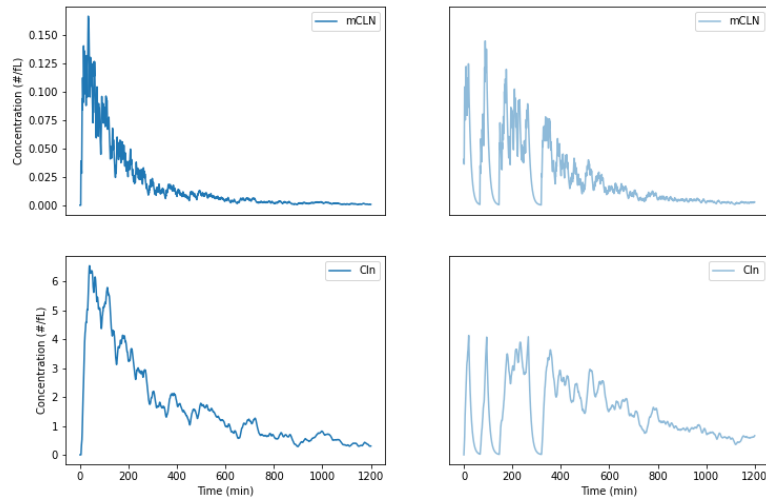


Figure 2.7: Single cell trajectory of mCLN and Cln concentration for a BGM simulation.

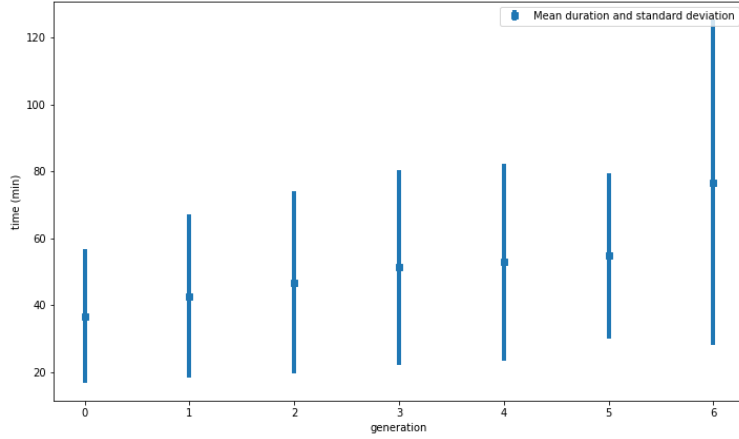


Figure 2.8: Population simulated with concentration based Cln threshold set to 4. Mean G1 duration and standard deviation vs. genealogical age.

Biomass dependent mRNA transcription

Lin et al. 2018 [11] argued that a cell size independent mRNA transcription is incompatible with the concentration homeostasis observed in growing cells. To overcome this they proposed a transcription model, based on the assumption that the number of RNA-polymerases (RNAPs) is rate limiting for transcription. They described the change of mRNA molecules m_i as a function of the number of (RNAPs) n and added a simple degradation kinetic.

$$\frac{d}{dt}m_i = k_p \cdot \Phi_i \cdot n - k_d \cdot m_i \quad (2.20)$$

To include the competition of active gene sites for the limited RNAPs they allocated only a fraction Φ_i of them to every gene i , according to their share on the total number of active gene sites.

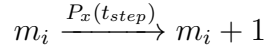
$$\Phi_i = \frac{g_i}{\sum_j g_j}$$

This notation could become very interesting for models with a high number of genes as in whole genome models or when transcription factors alter the activity of specific gene sites, as in more elaborate implementations of the cyclin network. The cyclin network in the BGM and the merged model consists only of two independent genes

CLN and CLB. The notation grants therefor no real advantage and Φ_i can be dropped in favor of an adjusted transcription rate k_p . Under the assumption that the RNAPs occupy a more or less constant fraction of the proteome, the number of RNAPs n can be replaced with the internal/metabolic biomass B_R :

$$\frac{d}{dt}m_i = k_p \cdot B_R - k_d \cdot m_i \quad (2.21)$$

This equation could be used to describe the average number of mRNA molecules in a cell with continuous transcription. However it is often assumed that transcription occurs not continuously but in bursts. The BGM implemented this as a chance P_x to add one more molecule of mRNA in every simulated time step



To include these bursts in eq. 2.21 an additional parameter k_{trans} can be included. In every time step it is either zero or one with a probability P_x .

$$\frac{d}{dt}m_i = k_{trans}(P_x) \cdot k_p \cdot B_R - k_d \cdot m_i \quad (2.22)$$

Unfortunately this model adjustment does not really solve the concentration issues of the BGM. In the last subsection of *Biomass function* an observation about the cell density B/V in the BGM was made. Within the BGM the cell density must change for growing cells, since eq. 2.19 can only be true for a constant structural biomass B_A . A similar condition can be found when looking at the concentration of the internal biomass B_R/V . It can not be constant for a growing cell either. Depending on how the allocation parameters k_R and k_A are chosen the density varies continuously. This has consequences for the mRNA concentration, when its production is scaled with B_R . In the standard parameter set of the BGM the ratio B_R/V is falling, as Spiesser et al. showed in Fig. 4C of their paper [14]. and the mRNA concentration instead of converging towards a stable value follows this trend.

Despite this incompatibility with the BGM the proposed adjustments can be meaningfully applied to the merged model. As described in the earlier section *Biomass function* it assumes a constant

cell density B/V and the concentration of the metabolic biomass B_R/V converges towards a stable value. Fig. 2.9 shows the temporal evolution of the concentration of Cln and its mRNA for a single cell. The left side shows a cell kept in G1 phase, the right side a cell that progressed through the cell cycle undisturbed. Both examples show clearly that concentration homeostasis is achieved apart from fluctuations due to the stochastic nature of the transcription process.

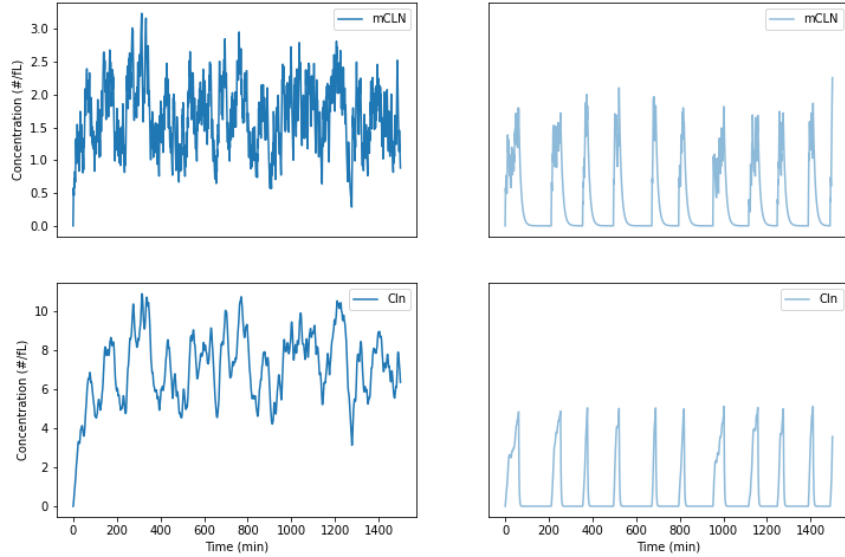


Figure 2.9: Single cell trajectory of mCLN and Cln concentration.

2.3 Comparison of MGM with BGM

In this section simulation results of the merged model are compared with key results of the BGM.

2.3.1 Mean cell size

The BGM demonstrated that the mean cell size of a cell population can converge to a stable attractor, even without limitations on the

size of individual cells. The merged model uses the same framework for cell cycle control and population simulations as the BGM, but different single cell growth dynamics. As fig. 2.10 B shows that cells in the merged model exhibit the same sigmoid volume trajectories as in the VGM (compare to Figure 1.5). According to eq. 2.1 the cells have a final volume, which is defined by the ratio of their rate constants for osmolyte uptake and consumption. Despite these differences the model shows similar behavior as the BGM. As shown in Figure 2.10 A the mean cell size of a population converges quickly after just a few generations.

It is experimentally observed that the mean cell size of a population is dependent on the cells' growth rate. The BGM allowed to tune the general growth rate of the simulated cells. The resulting populations reflected the experimental dependence of the mean cell size on that rate (Figure 1.4b). The merged model has a similar feature [1]. By increasing the uptake rate of osmolytes, but keeping the uptake to consumption ratio constant, the effective growth rate of the cells increases, whilst the final cell radius does not change (see Figure 2.10 B). In the following this is referred to as 'growth factor'. Figure 2.10 A shows that the mean cell volume of the populations simulated with the merged model is dependent on this growth factor.

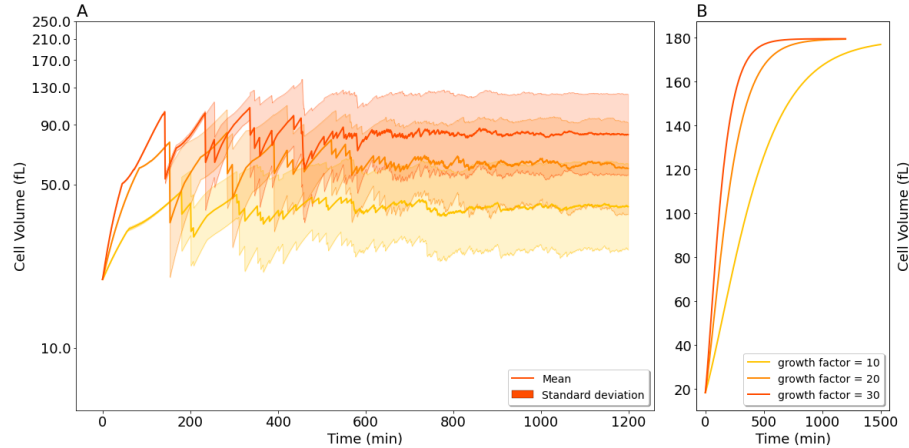


Figure 2.10: (A) Mean cell volume and standard deviation in log scale of simulated population for different growth factors. (B) Growth trajectory of single cells for different growth factors.

2.3.2 Size variability on the population level

In an initial paper Spießer et al. presented the BGM with only the G1 phase duration regulated by a simple signalling network. It consisted of a single proxy cyclin *Cln*. The G2 phase duration was fixed [14]. An extended version of the model was published in a second paper [13] with a variable G2 phase duration. This was motivated by in vivo experiments of the group. They found that while the mean cell volume of a population was clearly growth rate correlated, its size variability changed much less. Simulations of the original BGM with varied G2 phase durations indicated, that an adaptive G2 phase duration was needed to satisfy these experimental results [14]. This was realized by introducing a second proxy cyclin called *Clb*, which controlled a now variable G2 phase. Two implementations of the expanded model were compared. In the first version *Clb* was produced by mother and bud together, in the second only by the bud. The biological background for the latter were experimental observations that mRNA of the G2 phase cyclin *Clb2* was found mainly in the bud. Spießer et al. suggested that translation of this mRNA could be limited to the bud and its translational machinery. In the 'localized' model the amount of *Clb* could then function as a sensor for the metabolic capacity of the bud. When compared to the 'unlocalized' version, populations simulated with 'localized' *Clb* exhibited significantly smaller changes in size variability. This was in accordance with their experimental results, thus supporting their hypothesis of a 'localized' production of *Clb2*.

To test whether the merged model yields the same results, three implementations of the model were compared (Figure 2.11). They differed in the G2 phase being

1. regulated by *Clb*, produced in the bud
2. of fixed duration
3. regulated by *Clb*, produced in mother and bud

In all three cases the mean cell volume of the simulated populations increased with an increasing growth factor as expected and demonstrated for the 'localized' model in the former section. Their size variability was dependent on the growth factor as well. It was

clearly decreasing for the implementations with fixed G2 duration and with *Clb* produced by the mother and the bud. The 'localized' model followed the same trend, but was much more stable in this regard. This matches the results of the BGM. It seems that monitoring of the metabolic capacity of the bud through local production of *Clb* stabilizes the size variability of a population, not necessarily dependent on the underlying single cell growth model used.

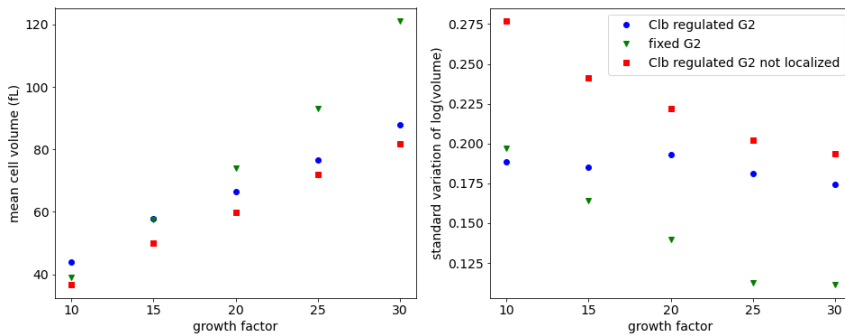


Figure 2.11: Results taken from last timepoint of population simulations. (A) Mean cell volume for different growth factors.(B) Standard deviation of cell volume for different growth factors.

2.3.3 Cell cycle timings

A strong feature of the BGM was the qualitative reproduction of cell cycle timings. Daughter cells have a particularly long G1 phase. This is commonly assumed to serve the purpose of maturing them further and let them grow to a considerable size before budding. The precise mechanism of this delay and especially how the critical size is sensed, is not fully understood. The BGM proposed that a critical threshold level of certain cyclins has to be reached, in order to trigger the genetic switch for a cell phase transition. The merged model uses the same approach for cell cycle control. Figure 2.12 shows the mean duration of the G1 phase over several generations for populations simulated with three different growth factors. All of them show a distinct drop after the first generation and a subsequent stabilization. The merged model reproduces the experimental data qualitatively and preserves this property of the BGM.

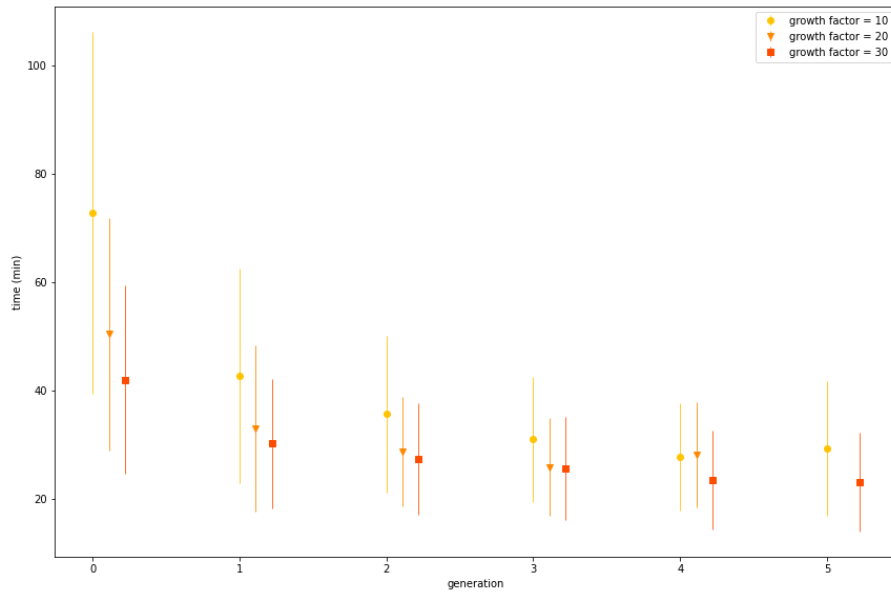


Figure 2.12: Results taken from last timepoint of population simulations. (A) Mean cell volume for different growth factors.(B) Standard deviation of cell volume for different growth factors.

Chapter 3

Discussion

Integrating the single cell model of Altenburg et al. [1] (VGM) into a population framework and adding an active cell cycle regulation, as the model of Spießer et al. [13] (BGM) provided it, seemed to be a promising project. The resulting merged model presented in this thesis combines various aspects of cellular biology, from thermodynamics and basic cell properties like density, to cell cycle regulation, modes of gene expression and population dynamics. Although coarse grained in its implementation, it suffices to qualitatively reproduce experimental observations, like cell cycle timings and size homeostasis on a population level.

In order to overcome their discrepancies and meaningfully merge them the BGM and VGM have been analyzed in depth. Efforts to expand the VGM to cover several generations revealed difficulties concerning the dynamics of osmolyte concentrations and turgor pressure, when the mother and the bud could exchange water and osmolytes. Although the observed phenomena are likely to be artefacts of the model, they could give an inside into why yeast cells have a limited replicative life span [16]. The analysis of the system behavior provided here could benefit further research of the model in this direction.

The concept of an auto catalytically growing biomass as in the BGM is incompatible with the finite cell growth of the VGM. To avoid this conflict a volume dependent biomass function has been derived, based on the assumption of a constant cell density. It allowed to incorporate the biomass dependent cell cycle regulation of the BGM into the VGM. Future experiments on the composition and density

of single cells for various volumes, growth rates and environments could be useful to improve and correct the model here. Despite these adjustments the simple second order reaction kinetic used for the cyclins should lead to exponential cell growth, when applied to ribosomes. This inconsistency within the merged model remains to be solved.

An analysis of mRNA concentrations in the BGM showed their strong dilution, contrary to experimental observations [15]. Based on a gene expression model by Lin et al. [11] an adjustment of the model for stochastic transcription has been proposed. Even though not functional for the BGM it is applicable to the merged model and produces stable mRNA concentrations.

Despite their different models for cell growth a comparison of the merged model with the BGM showed great congruence in key results. This suggest a robustness of the underlying ideas of the BGM against the chosen growth behavior of the single cells. Namely the scaling of the cyclin production with an increasing metabolic capacity of the cell seems to be crucial to explain the differences in G1 phase durations between mother and daughter cells.

Linking the osmolarity of the growth medium directly with the cell growth dynamics could allow some new interesting *in silico* experiments. Goldenbogen et al. simulated osmotic shocks for single cells with their VGM. These experiments could be repeated for whole populations to study the effect on overall growth. In similar simulations the osmolarity of the growth medium could be changed to study the effects of starvation on a population. This could be done by directly tuning the external osmolarity or by introducing the consumption of osmolytes from a finite reservoir. In fact contrary to intuition a simple reduction of the external osmolyte concentration due to nutrient consumption would *induce* cell growth according to both the merged model and the VGM. A more detailed implementation of key osmolytes and basic metabolic processes could shed light on the interplay of osmotic pressures and the cellular need for nutrients in the context of growth.

Bibliography

- [1] T. Altenburg, B. Goldenbogen, J. Uhlendorf, and E. Klipp. “Osmolyte homeostasis controls single-cell growth rate and maximum cell size of *Saccharomyces cerevisiae*”. *npj Systems Biology and Applications* 5.1 (2019). URL: <http://dx.doi.org/10.1038/s41540-019-0111-6>.
- [2] W. W. Baldwin and H. E. Kubitschek. “Buoyant density variation during the cell cycle of *Saccharomyces cerevisiae*”. *Journal of Bacteriology* 158.2 (1984), pp. 701–704.
- [3] F. Barber, A. Amir, and A. W. Murray. “Cell-size regulation in budding yeast does not depend on linear accumulation of Whi5”. *Proceedings of the National Academy of Sciences* 117.25 (2020), p. 202001255.
- [4] J. Cui. “Visualization of the Budding Yeast Cell Cycle Visualization of the Budding Yeast Cell Cycle” (2017).
- [5] J. M. Enserink and R. D. Kolodner. “An overview of Cdk1-controlled targets and processes”. *Cell Division* 5 (2010), pp. 1–41.
- [6] N. Filigheddu, V. F. Gnocchi, M. Coscia, M. Cappelli, P. E. Porporato, and R. Taulli. “The size of the nucleus increases as yeast cells grow”. *Molecular biology of the cell* 18.December (2007), pp. 986–994.
- [7] C. Garmendia-Torres, O. Tassy, A. Matifas, N. Molina, and G. Charvin. “Supplementary: Multiple inputs ensure yeast cell size homeostasis during cell cycle progression”. *eLife* 7 (2018).
- [8] L. H. Hartwell and M. W. Unger. “Unequal division in *Saccharomyces cerevisiae* and its implications for the control of cell division”. *The Journal of Cell Biology* 75 (1977), pp. 422–435.
- [9] T. Hunter and M. Karin. “The regulation of transcription by phosphorylation”. *Cell* 70.3 (1992), pp. 375–387.
- [10] O. Kedem and A. Katchalsky. “Thermodynamic analysis of the permeability of biological membranes to non-electrolytes”. *BBA - Biochimica et Biophysica Acta* 27.C (1958), pp. 229–246.
- [11] J. Lin and A. Amir. “Homeostasis of protein and mRNA concentrations in growing cells”. *Nature Communications* 9.1 (2018). URL: <http://dx.doi.org/10.1038/s41467-018-06714-z>.

- [12] E. Noguchi and M. C. Gadaleta. *Cell Cycle Controll.* Vol. 1170. 2014, pp. 99–111.
- [13] T. W. Spiesser, C. Kühn, M. Krantz, and E. Klipp. “Bud-Localization of CLB2 mRNA Can Constitute a Growth Rate Dependent Daughter Sizer”. *PLoS Computational Biology* 11.4 (2015), pp. 1–24.
- [14] T. W. Spiesser, C. Müller, G. Schreiber, M. Krantz, and E. Klipp. “Size homeostasis can be intrinsic to growing cell populations and explained without size sensing or signalling”. *FEBS Journal* 279.22 (2012), pp. 4213–4230.
- [15] X. M. Sun, A. Bowman, M. Priestman, F. Bertaux, A. Martinez-Segura, W. Tang, C. Whilding, D. Dormann, V. Shahrezaei, and S. Marguerat. “Size-Dependent Increase in RNA Polymerase II Initiation Rates Mediates Gene Expression Scaling with Cell Size”. *Current Biology* 30.7 (2020), 1217–1230.e7. URL: <https://doi.org/10.1016/j.cub.2020.01.053>.
- [16] R. Zadrag-Tecza, M. Kwolek-Mirek, G. Bartosz, and T. Bilinski. “Cell volume as a factor limiting the replicative lifespan of the yeast *Saccharomyces cerevisiae*”. *Biogerontology* 10.4 (2009), pp. 481–488.

Chapter 4

Appendix

4.1 Model species, parameters and equations

The tables below contain all species, parameters and equations used in the MGM.

Species	description
V_{os}	Osmolitically active volume, increases with water influx
V_b	Volume of solid components, proportional to reference volume
r	Total cell radius
R_{ref}	Reference Radius, radius of relaxed cell without elastic expansion (grows by plastic expansion)
Π_t	Tugor pressure
c_i	Inner osmolyte concentration
B_R	internal biomass
B_A	structural biomass
B	total biomass
$mCLN$	mRNA of the G1 proxy cyclin Cln
$mCLB$	mRNA of the S/G2 proxy cyclin Clb
Cln	proxy cyclin regulating length of the G1-phase
Clb	proxy cyclin regulating length of the S/G2-phase

parameter	specification	G1	S/G2/M
k_{pCln}	production rate Cln ($\text{min}^{-1} \cdot \text{mol}^{-1}$)	1	0
k_{pCln}	production rate Cln ($\text{min}^{-1} \cdot \text{mol}^{-1}$)	0	1
k_{deg}	degradation rate of cyclins and mRNA (min^{-1})	0.1	0.1
P_x	probability of mRNA transcription (min^{-1})	0.4	0.4
$threshold$	concentration of Cln (G1)/ Clb (G2) needed to trigger phase transition	5	5

parameter	description	value	unit
V_{os}^0	Initial volume of solid components	10	μm^3
c_i^0	Initial inner osmolyte concentration	319.17	$ mM$
Π_t^0	Initial tugor pressure	$2.0 \cdot 10^5$	$ Pa$
c_e	Outer osmolyte concentration	240.0	$ mM$
R	Ideal gass constant	8.314	$\frac{J}{mol \cdot K}$
T	Temperature	303	$ K$
L_p	Membrane water permeability	$1.19 \cdot 10^{-6}$	$\frac{\mu m}{s \cdot Pa}$
Π_{tc}	Critical tugor pressure	$2.0 \cdot 10^5$	$ Pa$
d	Cell wall thickness	0.115	$ \mu m$
Φ	Cell wall extensibility	$1.0 \cdot 10^{-4}$	$\frac{1}{s \cdot Pa}$
E	Young's modulus	$3.44 \cdot 10^6$	$ Pa$
k_{uptake}	Osmolyte uptake rate constant	5.25	$\frac{mM}{s \cdot \mu m^2}$
$k_{maintenance}$	constant osmolyte consumption	4.5	<i>arb.unit</i>
ρ_{cell}	cell density	0.5	g/fL
ρ_b	biomass density	1.1	g/fL

ODE
$\frac{d}{dt} V_{os} = -L_p \cdot A \cdot (\Pi_t + \Pi_e - \Pi_i)$
$\frac{d}{dt} V_b = \frac{k_D}{k_b - k_D} \cdot V_{os}$
$\frac{d}{dt} r = \left(\frac{3}{12\pi} \cdot \frac{k_b}{k_b - k_D} t \right)^{\frac{1}{3}} \cdot \frac{dV_{os}}{V_{os}^{\frac{2}{3}}}$
$\frac{d}{dt} R_{ref} = \frac{\Phi \cdot R_{ref} \cdot r}{2 \cdot d} \cdot f_1(\Pi_t)$
$\frac{d}{dt} \Pi_t = \frac{2 \cdot E \cdot d}{1 - \nu} \cdot \left(\frac{dr}{r^2} - \frac{\dot{R}_{ref}}{R_{ref}} \cdot \frac{1}{r} \right) - \frac{dr}{r} \cdot \Pi_t$
$\frac{d}{dt} c_i = 3 \cdot \frac{k_{uptake}}{r} - k_{maintenance} - 3 \cdot \frac{dr}{r} \cdot c_i$
$\frac{d}{dt} B_A = k_A \cdot 8 \cdot \pi \cdot R_{ref} \cdot \dot{R}_{ref}$
$\frac{d}{dt} B_R = \frac{k_D \cdot k_b}{k_b - k_D} \cdot \dot{V}_{os} - \dot{B}_A$
$\frac{d}{dt} B = \dot{B}_A + \dot{B}_R$
$\frac{d}{dt} mCLN = B_R \cdot f_2(P_x) - k_{deg} \cdot mCLN$
$\frac{d}{dt} mCLB = B_R \cdot f_2(P_x) - k_{deg} \cdot mCLB$
$\frac{d}{dt} Cln = k_{pCln} \cdot mCLN \cdot \frac{B_R}{V} - k_{deg} \cdot Cln$
$\frac{d}{dt} Clb = k_{pClb} \cdot mCLB \cdot \frac{B_R}{V} - k_{deg} \cdot Clb$
$f_1(\Pi_t) = \max(\Pi_{tc} - \Pi_t, 0)$
$A = 4 \cdot \pi \cdot r^2$
$f_2(P_x)$ Is either 1 or 0 in every time step with probability P_x .

4.2 Model code

All simulation results of the merged model have been generated using Python3 in the Jupyter environment. A GitHub repository with a working version of the code can be found under https://github.com/LPolczynski/Bachelor_Thesis. To run the code the following packages are necessary:

- numpy
- scipy

- joblib
- copy
- time
- math
- pickle
- datetime
- matplotlib
- pylab
- os
- shutil